59th ILMENAU SCIENTIFIC COLLOQUIUM
Technische Universität Ilmenau, 11 – 15 September 2017
URN: urn:nbn:de:gbv:ilm1-2017iwk-117:6

FPGA-BASED SIGNAL PROCESSING OF A HETERODYNE INTERFEROMETER

Oliver Dannberg[1], Ingo Ortlepp[1], Eberhard Manske[1]

[1]Technische Universität Ilmenau, Institute of Process Measurement and Sensor Technology

ABSTRACT

A heterodyne interferometer and a data acquiring algorithm have been developed to measure the movement of a mirror in one dimension, as well as its rotation around two axis. The interferometer uses spatially separated beams to reduce periodic optical non-linearities, furthermore the optical set-up was designed for low drift, few number of optical elements and easy adjustment. The FPGA-based signal processing is based on an undersampling technique with the aim to minimise the calculation effort. The working principles of the interferometer and the electronics are described and their remaining non-linearities are investigated. Finally, the z-position, the tip and tilt angle of a planar stage are measured with the described system as an example of use.

Index Terms - interferometer, heterodyne, FPGA, non-linearities, undersampling

1. INTRODUCTION

Interferometers in general are used in high-precision machines such as coordinate measuring machines, wafer steppers and for calibration [7]. For length measurement tasks with demands for very high accuracy and very low drift, heterodyne interferometers (HIF) are of great importance. In contrast to homodyne interferometers, HIF are insensitive to signal intensity and ambient light variations due to the constantly alternating signal of a HIF. This makes them perfectly suitable for slow varying movements such as drift measurements. Therefore, they are especially used for displacement measurement of precision stages [8] as well as sensor calibration.

However, due to the complex signal processing, requiring numerous operations (mixing, filtering) on high frequency signals, HIF require high-performance Hardware for A/D-conversion and computation which makes them comparatively expensive. Furthermore, in interferometers with coaxial beam design, optical non-linearities expend the bulk of the measuring uncertainty.

To overcome those drawbacks, a simple plane mirror interferometer set-up without optical non-linearities as well as efficient signal processing algorithms, requiring less powerful hardware, were developed in this project.

2. STATE OF THE ART

Heterodyne interferometers of the classic Michelson design with coaxial beams suffer from leakage beams which result from optical parts imperfections (reflections at glass surfaces, incomplete polarisation separation of beam splitters), inevitable leading to frequency mixing and periodic optical non-linearities. Figure 1 shows the leakage beams occurring in a coaxial set-up.

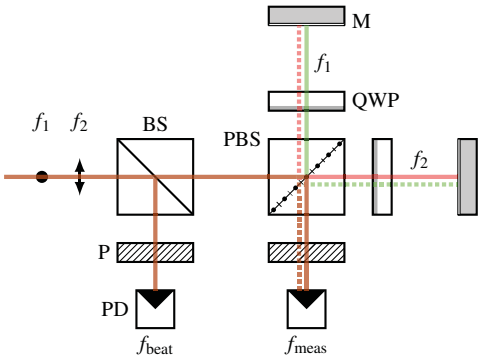

Figure 1: *Coaxial heterodyne interferometer with imperfect polarisation splitting, leading to leakage beams (dotted) and thus optical non-linearities.*
BS:beam splitter, PBS: polarising beam splitter, P: polariser, PD: photodiode, QWP: quarter wave plate, M: mirror.

Several attempts were made to avoid this frequency mixing by spatially separating the two heterodyne frequencies instead of using two coaxial beams with orthogonal polarisation.

In [9] an interferometer using a retro reflector (corner cube) as measuring reflector is described (fig. 2). The heterodyne frequencies enter the beam splitter spatially separated and their orientation is flipped at the measuring reflector to overlap the beams. As this system relies on the beam shift induced by the retro reflector, it is not suitable for plane mirror applications.

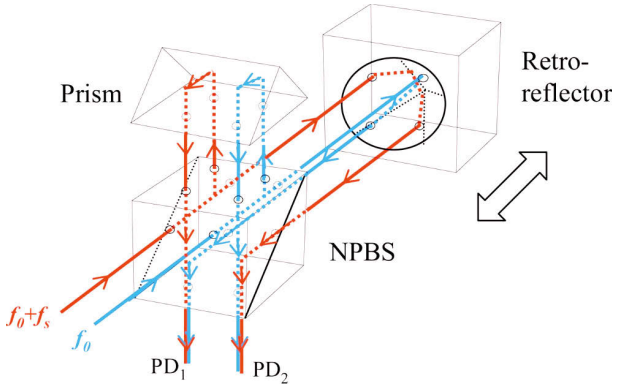

Figure 2: *Set up of a heterodyne interferometer with spatially separated beams using a retro reflector as measuring reflector and to unite the two beams [9].*
NPBS: non polarising beam splitter, PD: photo diode

Another attempt with separated beams is shown in [10]. There, a plane mirror double pass interferometer is described. A right angle prism is used for generating the second pass and the beams are finally united using a PBS. The set-up of this interferometer is, however, a single axis set-up, not suitable for (multi axis) angular measurements. The Delft-PM interferometer described in [11] is using a similar single axis set-up with corner cubes for beam shifting and a plane mirror as measuring reflector.

The design proposed by [12] is a plane mirror set-up which is in principle applicable for multi axis interferometers. However, the separate splitting of the two heterodyne frequencies makes this approach impractical for numerous measurement axis due to the large number of necessary beam adjustments.

3. INTERFEROMETER SETUP

3.1. Optics

The characteristic of the HIF designed in this project is the consequent spatial separation of the two heterodyne wavelengths: both wavelengths are generated by two PLL-coupled He-Ne-lasers [13] and transmitted to the HIF by separate optical fibres. Inside the HIF, both beams propagate

parallel with a distance of 4 mm and are not united before completely passing the whole interferometer. With this approach of spatial separation, unwanted interactions of the beams (frequency mixing) are effectively suppressed. This results in very low periodic optical non-linearities in the pico-metre-range. The HIF designed in this project is a 3-beam interferometer for measuring displacement z and two rotation angles φ_x, φ_y.

Typically, a fraction of both heterodyne frequencies is coupled out before the interferometer to obtain the reference signal (fig. 1). This way, influences of the following optical parts as well as local differences in the refractive index inside the beam path remain unrecognised. To compensate these influences, an additional interferometric axis was included, which passes the HIF in the same way the measurement beams do. Thus, the present influences of the optical parts and the like equally take effect on the measurement and reference beams and are therefore compensated as best as possible.

As a first step, the two heterodyne frequencies are split in four beam pairs where three pairs serve as the measuring beams and one pair as a reference for the beat frequency. The splitting assembly (fig. 3) is designed for minimal adjustment necessity. When f_1 and f_2 enter the set-up parallel, they will stay parallel throughout the whole optical assembly. Thus, it is sufficient to adjust the beams pairwise at the exit of the splitter to compensate the angular tolerances of the beam splitters and mirrors.

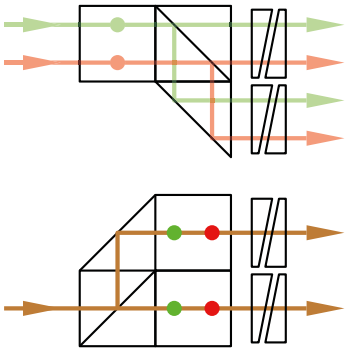

Figure 3: *Beam splitting of the 4 interferometer axes. The adjustment complexity is reduced, as f_1 and f_2 are adjusted simultaneously by a pair of wedge plates.*
Upper picture: side view, lower picture: top view.

The four beam pairs are afterwards passed to the actual interferometer. As they are orthogonally polarised, the frequencies are separated at the main polarising beam splitter. After passing the quarter wave plates they hit a fixed or the measuring mirror respectively and reach the lower beam splitters. There, f_2 is shifted parallel to overlap with the f_1-beam. The linear polariser is used to match the polarisation of the frequencies to enable their interference.

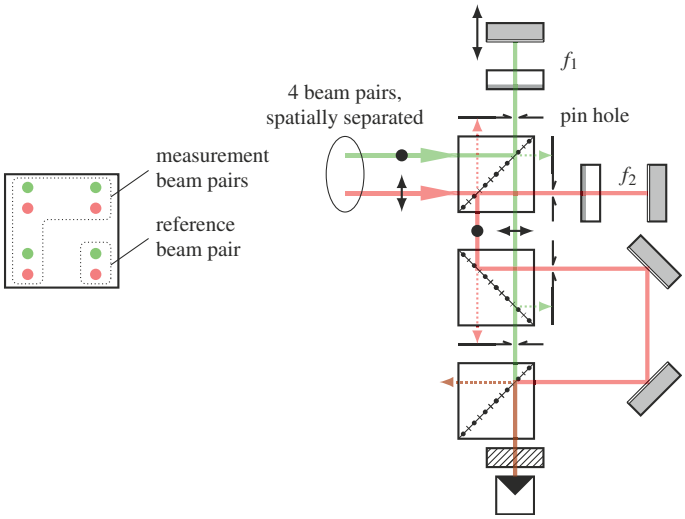

Figure 4: *Left side: Beam arrangement in the interferometer (view along beam propagation). Three beam pairs serve as measuring beams for determining the mirror position in 3 axes (z, φ_x, φ_y). The fourth beam pair serves as a reference (beat frequency).*
Right side: Beam path in a HIF with separated beams (one axis). The heterodyne frequencies (green, red) are kept separated until short before the photodiodes, so leakage beams (dotted) have no effect on the related parallel beam, avoiding unwanted frequency mixing and optical non-linearities. For the reference beam pair, the f_1-mirror is fixed, representing the beat signal.
Advantage of this set-up: The optical paths are nearly identical for measurement and reference pairs (same glass length, same path in air with small displacement).

To reduce the number of optical elements, all beams of f_2 are shifted at the same time in the same direction (fig. 4) to unite both heterodyne frequencies. This group wise shifting also reduces the necessary adjustments as the beams run parallel anyway.

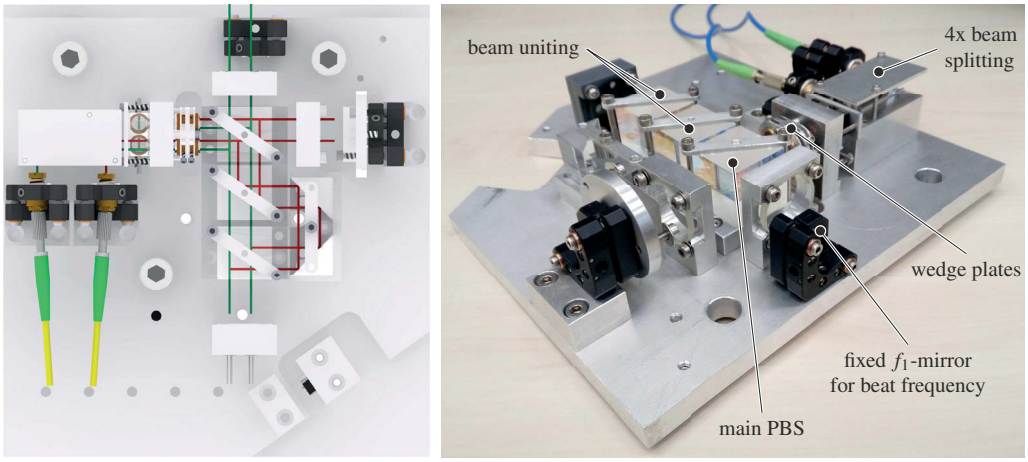

Figure 5: *Left side: CAD model of the HIF with beam layout. Two beam pairs are visible, two more are located beneath.*
Right side: Interferometer with fixed f_1-mirror for the beat frequency. The three remaining beams run aside that mirror, hitting the actual measuring mirror (not shown).

4. SIGNAL PROCESSING

The heterodyne interferometer, which is described in this paper, uses two laser beams with a difference frequency of $f_1 - f_2 = f_0 = 4\,\text{MHz}$. A splitting assembly (fig. 3) produces four beam pairs of which one serves as a reference. The remaining three beam pairs, however, are reflected by a movable measurement mirror. The following procedure describes the evaluation process that is individually done for all three measurement signals.
If the measurement mirror moves, the detected frequency in the measurement signal is shifted by the Doppler effect $f_{meas} = f_1 - f_2 + f_d$. The phase shift between reference and measurement signal depends linearly on the mirror position (Δx) and needs to be determined. This is realized with the "RedPitaya" [3], which is a System-On-a-Chip with an integrated FPGA, CPU, two A/D-converters and various output ports. It determines the phase shift by undersampling both signals with an undersampling factor of $r = \frac{f_{signal}}{f_{sample}} = 4$. Since the sampling rate is below the Nyquist frequency $f_{sample} < \frac{f_{beat}}{2}$, an aliasing effect occurs that shifts the frequency band $f_0 \pm f_d$ to the baseband [4]. If the frequency of the signal shifts below or above f_0 , the difference frequency is detectable in the undersampled signal. In order to decide whether the signal is in-

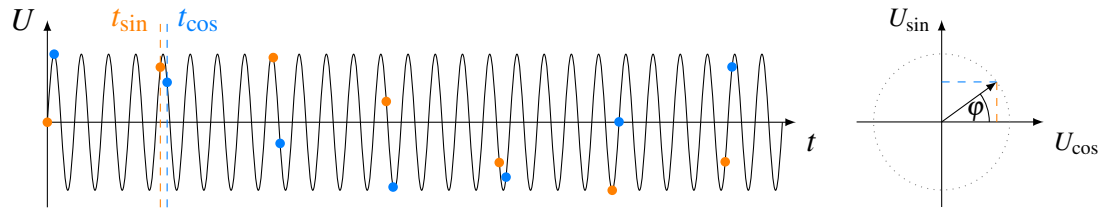

(a) *Undersampling* **(b)** *Vector diagram*

Figure 6: *(a) shows a signal (black) that is undersampled with a factor of $r = 4$. Each time, the intensity of the signal is detected at two certain points (orange=sine and blue=cosine). These are shifted by a quarter period (90°) of the original signal. The vector diagram (b) illustrates the determination of the phase for one pair of values.*

creasing or decreasing, two points with a 90° phase shift are acquired each time (sine and cosine). Fig. 6a shows an example of undersampling a signal (black) with a slightly increased frequency. The orange and blue points represent the undersampled sine and cosine signal. Each pair of values is used to determine the phase of the incoming signal in relation to the undersampling rate $\varphi = \arctan(\frac{U_{\sin}}{U_{\cos}})$. This is exemplary visualized for an acquired value pair in fig. 6b. If the frequency of the signal doesn't exactly match the undersampling frequency, the phase starts to rotate. However, this is compensated by calculating the difference between the phase of the beat and measurement signal $\varphi = \varphi_{beat} - \varphi_{meas}$.
The calculation of each phase is realized with an iterative CORDIC algorithm [5] with a range of 360°. An excess of this limit produces an overflow and thus results in a jump. An example of this effect is given in top of fig. 7.

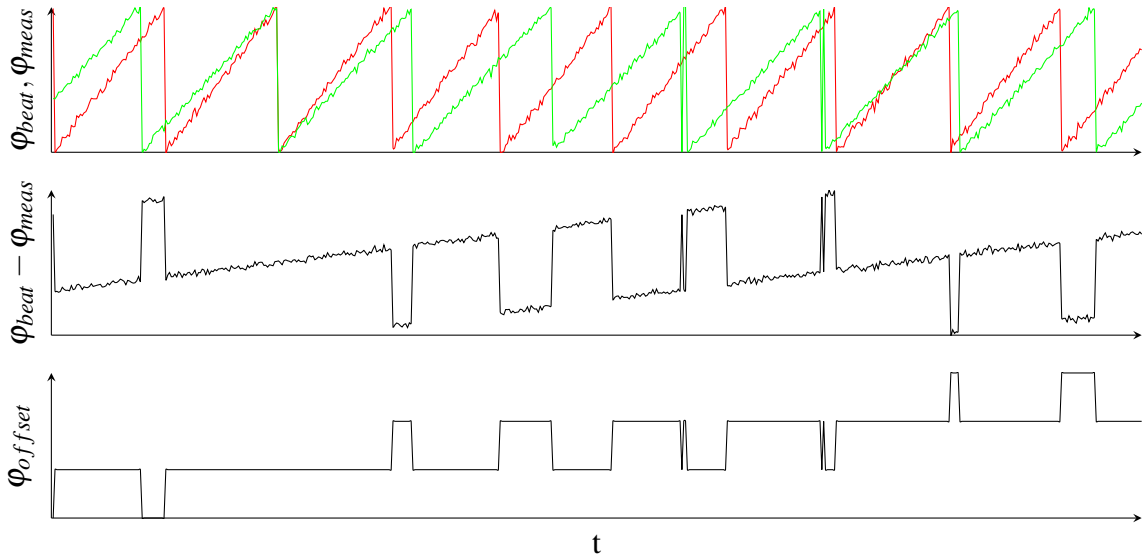

Figure 7: *The incoming beat and measurement signal with a constant but unequal increase, as well as noise (top). Overflowing of the phases result in jumps that are detectable in the phase difference, too (middle). The FPGA compensates the jumps with an offset value (bottom).*

Since the signals increase with different gradients, the jump frequency is different, too. All jumps of both signals are also present in the difference signal which is shown in the middle of fig. 7). The only exception is a jump of both signals at the same time which results, depending on the jumping direction, in a compensation or accumulation of the jumps. This is the case for the second edge of both signals. In order to detect these jumps, the FPGA compares each value of the phase difference with the previous one. If this value exceeds a specific threshold, the FPGA changes an offset value to compensate the jump. Due to the gradient of the phase difference and the noise level, the threshold is slightly below the actual jump height. The last diagram in fig. 7 shows the corresponding offset for the incoming signals. The sum of the offset and the phase difference represents the mirror position without jumps.
In order to increase the signal-to-noise ratio, the signal passes a digital low pass filter that is realized as a FIR filter with 2048 coefficients in a symmetric Hamming-window [6]. The remaining noise is $\approx 1\,\%$ of the initial noise level.

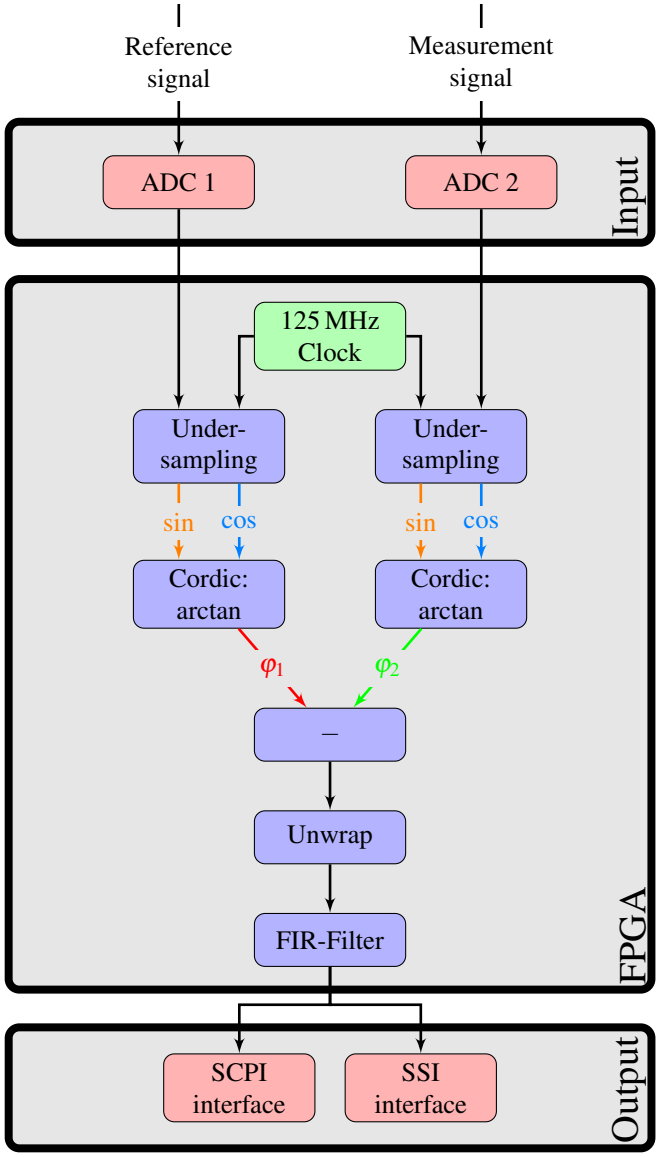

Figure 8: *Illustration of the data flow inside the RedPitaya. Both signals are acquired separately with an A/D-converter. The internal clock of the RedPitaya serves as a time reference to undersample both signals. A CORDIC based algorithm transforms the resulting sine and cosine signals into an angle. The jumps of the difference signal are detected and compensated. Afterwards, the signal is filtered by a FIR-Filter which reduces the noise. Two possible output interfaces enable the user to transfer the data.*

However, the filter causes a delay of $\approx 1\,\mathrm{ms}$ and reduces the dynamics of the system by cutting off the higher frequencies. This trade-off is acceptable, since the mirror movement is relatively slow. The reconfigurable FPGA enables the user to easily change the filter coefficients, if required. Each step of the signal processing within the FPGA is summarized in fig. 8.

4.1. Limitations and non-linearities

The principle of undersampling is an efficient way of data acquisition with low hardware requirements. However, the range of the measurable frequency and thus the speed of the measurement mirror is limited. The maximal frequency difference must be below the Nyquist frequency which leads to $\Delta f_{max} > \frac{f_0}{r \cdot 2}$. Assuming a symmetrical frequency band, the maximal speed of the mirror is $v_{max} = \pm 158\,\mathrm{mm\,s^{-1}}$. This limit could be raised by choosing a lower undersampling factor which, however, would increase the hardware requirements.
Another disadvantage of the undersampling principle is the appearance of periodical non-linearities. One can distinguish two categories of non-linearities: dynamic and static. Both occur,

if the time difference between the sine and cosine detection is not exactly 90° of the current signal frequency. The dynamic non-linearities are due to the frequency shift during the mirror movement. Since the movement doesn't effect the beat signal, the dynamic non-linearities do only effect the measurement signal. If the time difference does not match a quarter period of the beat signal, static non-linearities occur regardless of the mirror movement. Fig. 9 illustrates how non-linearities influence the measurement. The green plot shows a signal that has been detected with a 90° time difference in a vector diagram. However, the red line shows the measurement

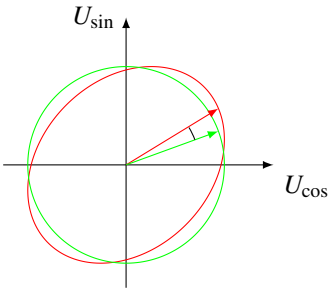

Figure 9: *A vector diagram visualizes the sine and cosine values of two different signals. In case of the green line, the phase shift between the detections is exactly 90° of the current signal. However, the red line represents a measurement with a phase shift that is less than a quarter period. The resulting non-linearity directly influences the measurement of the interferometer and is periodically repeated.*

of the same signal with a time difference that is lower than 90°. The colored arrows represent the pointers of both measurements at one certain moment. A black line indicates the current deviation angle that is due to the non-linearity of the red signal. The angle deviation oscillates with a period of $\lambda/2$ and directly influences the measurement of the interferometer.

5. EXPERIMENTAL RESULTS

After completion of the optical and electronic subsystems, the HIF was investigated widely. This includes the separate verification of the electronics as well as the overall system. In the experiments, the focus was to determine the remaining non-linearities.

5.1. FPGA

In order to avoid static non-linearities, the measurement requires an ideal time difference between sine and cosine detection of $\Delta t_{ideal} = \frac{1}{4 \cdot f_0} = 62.5\,\text{ns}$ (see section 4.1). However, the real system uses the integrated clock of the FPGA as a time reference. It has a frequency of 125 MHz which allows for a time difference of $\Delta t_{real} = 64\,\text{ns}$. The following fig. 10 shows the simulated amplitude of the non-linearities, depending on the speed of the mirror. The dynamic non-linearities increase linear with an approximate rate of $64.5\,\frac{\text{nm}}{\text{m/s}}$. However, the deviation at zero velocity

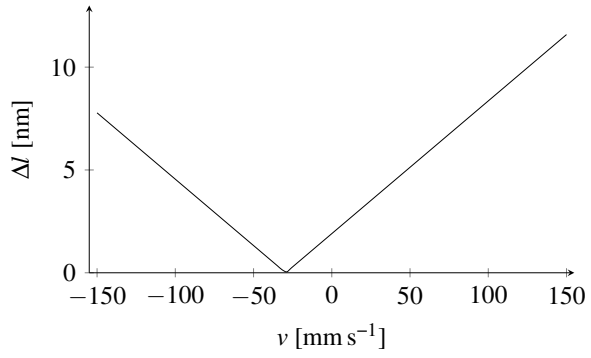

Figure 10: *Simulated deviation of the HIF, depending on the velocity of the measurement mirror. The value increases linearly with a rate of* $64.5\,\frac{\text{nm}}{\text{m/s}}$ *and a horizontal offset of* $29.5\,\text{mm}\,\text{s}^{-1}$.

represents the static non-linearities of $\approx \pm 1\,\mathrm{nm}$. If the measurement mirror moves with a speed of $29.5\,\mathrm{mm\,s^{-1}}$ away from the HIF, the frequency of the signal matches with the detection timing. Theoretically, the non-linearities are zero during this movement.

5.2. Interferometer

For determining the optical periodic non-linearities, the measuring mirror was fixed on a brass rod. The rod was heated by a winded wire so the measuring mirror was moved by the thermal expansion of the rod. To eliminate electrical influences, the actual measurements were carried out with the heater switched off, in the cooling phase of the rod. As the thermal shrinkage can be considered free from periodic non-linearities, any detected periodic non-linearities can be assigned to the interferometer. The three interferometer axes were measured separately for determining the length non-linearities and also pairwise for the angular non-linearities. In this case the brass rod drove a lever to which to measuring mirror was fixed (fig. 11).

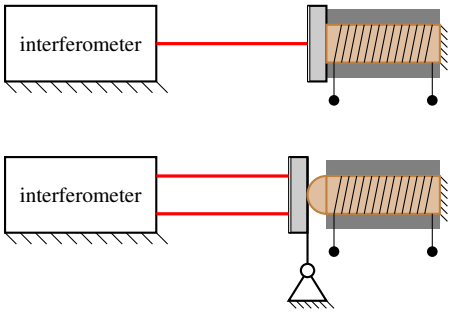

Figure 11: *Determining the periodic optical non-linearities of the HIF. The measuring mirror is driven by a heated brass rod (brown), using the thermal expansion as a periodicity-free motion. To reduce influences from the environment, the rod is thermally isolated (gray).*
Upper view: length measurement
Lower view: angular measurement

The identified optical non-linearities are considerably smaller than 1 nm in the proximity of $\lambda/2$ and $\lambda/4$, The following figure 12 shows an example measurement for one interferometer axis.

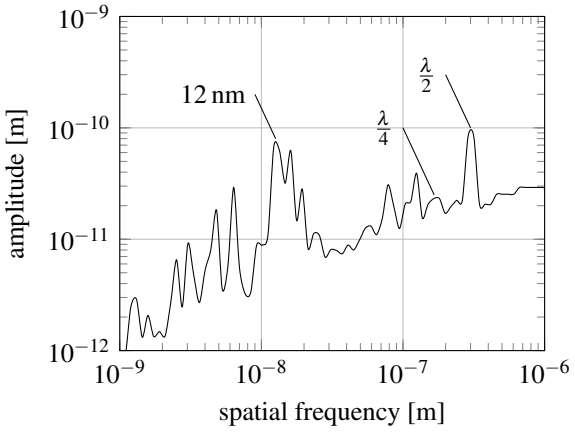

Figure 12: *Periodic non-linearities of the interferometer at a mirror velocity of approx. $5\,\mu m\,s^{-1}$. The main peaks are at $\lambda/2$ (optical non-linearity) and 12 nm which might result from acoustic influences.*

The investigations with this interferometer set-up were all carried out using photodiodes as optical receivers. Additionally the interferometer was build up as full-fibre assembly. By supplying the heterodyne frequencies and returning the interferometer signals with fibres, it is possible to realise a completely passive interferometer assembly. This is especially useful for e.g vacuum use, as there is no power dissipation inside the interferometer and hence no heat transfer to the measuring volume. Furthermore the optical signal transmission is less susceptible

to interference than an electrical one. The investigations on the full-fibre version of the interferometer have shown that coupling the optical signals into multimode fibres and placing the photodiodes in sufficient distance has no significant effects on the measuring signal (amplitude, noise, non-linearity) and hence the full-fibre set-up can be used as needed.

5.3. Measurements in planar stage

After investigating the interferometer, it was installed into a planar stage to measure the height and horizontal angular deviations of the slider as a proof of work. The planar stage consists of a granite base and a slider which is guided by three air bearings with active height control [14]. The vertical rotation angle is controlled by three pairs of coils and two interferometers (x, y, φ_z). The following figure 13 shows the planar stage and the interferometer.

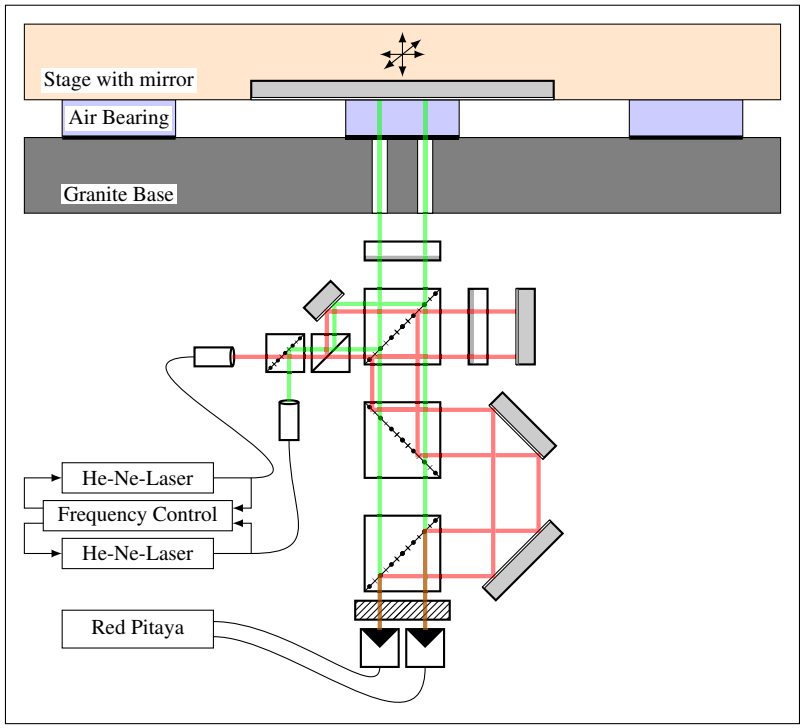

Figure 13: *Planar stage with air guided slider and 3 axis heterodyne interferometer. The HIF is used to measure the height and angular deviations of the slider to allow for offline correction or active height control as shown in [14].*

After the adjustment of all components, first measurements at rest were made to check the function and stability of the system. After that the (circular) movement range of the slider was scanned and the z-position as well as the angular deviations φ_x and φ_y were observed. The following figure 14 shows the height deviation of the planar stage slider.

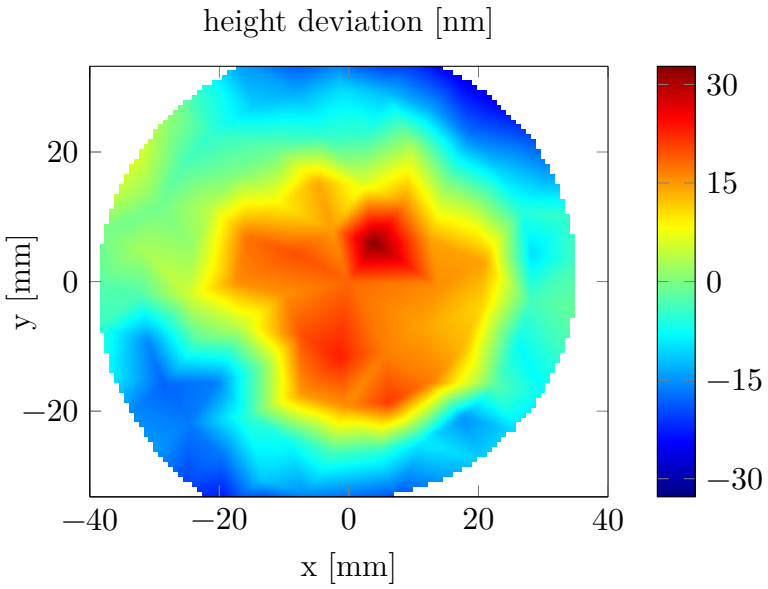

Figure 14: *Height deviation of the planar slider, measured with the developed heterodyne interferometer. The flatness deviation is 65 nm in the whole moving range.*

6. CONCLUSION and OUTLOOK

A three axis heterodyne interferometer and data acquiring algorithm have been developed and investigated. The interferometer is designed to be free from optical periodic non-linearities and to require less optical parts and adjustment effort. This is achieved by separating the two heterodyne frequencies throughout the whole interferometer and bring them to interference not until they reach the photoelectrical detectors. The beam arrangement inside the interferometer is optimised for an equal optical path for all beam pairs as well as easy adjustment. Measurements were taken to determine the residual periodic non-linearities for the interferoemter and for the electronics. The periodic non-linearities of the system are smaller than 0.1 nm at $\lambda/2$ and its integer fractions. Finally, as a proof of work, the whole measuring system was installed in a planar stage to determine the angular and height deviation of its slider. It could be shown that height deviations smaller than 100 nm could be easily measured.

Future work will include further optical improvements (even less optical parts) while at the same time increasing the resolution by a double-pass version of the interferometer. Furthermore, the photodiode amplifiers have to be optimised (speed, noise) for the used beat frequency of 4 MHz.

REFERENCES

[1] Frank C Demarest. "High-resolution, high-speed, low data age uncertainty, heterodyne displacement measuring interferometer electronics". In: *Measurement Science and Technology* 9.7 (1998), p. 1024.

[2] Paul Köchert et al. "A fast phase meter for interferometric applications with an accuracy in the picometer regime". In: (2011). URL: http://www.degruyter.com/view/j/teme.2014.81.issue-6/teme-2014-0404/teme-2014-0404.xml.

[3] 2016 StemLabs. *Test & Measurement applications running on a credit card sized SoC (FPGA+CPU)*. June 13, 2017. URL: https://redpitaya.com/.

[4] Arthur Kohlenberg. "Exact Interpolation of Band-Limited Functions". In: *Journal of Applied Physics* 24.12 (Dec. 1953), pp. 1432–1436. DOI: 10.1063/1.1721195. URL: https://doi.org/10.1063%2F1.1721195.

[5] Jack E Volder. "The CORDIC trigonometric computing technique". In: *IRE Transactions on electronic computers* 3 (1959), pp. 330–334.

[6] Belle A Shenoi. *Introduction to digital signal processing and filter design*. John Wiley & Sons, 2005.

[7] E Jäger et al. "Nanomessmaschine zur abbefehlerfreien Koordinatenmessung (Nano Measuring Machine for Zero Abbe Offset Coordinate-measuring)". In: *tm Technisches Messen Plattform für Methoden, Systeme und Anwendungen der Messtechnik* 67.7-8/2000 (2000), p. 319. DOI: 10.1524/teme.2000.67.7-8.319. URL: http://www.degruyter.com/view/j/teme.2000.67.issue-7-8_2000/teme.2000.67.7-8.319/teme.2000.67.7-8.319.xml.

[8] Jens Fluegge and Rainer G. Koening. "Status of the nanometer comparator at PTB". In: *Recent Developments in Traceable Dimensional Measurements*. Ed. by Jennifer E. Decker and Nicholas Brown. SPIE, Oct. 2001. DOI: 10.1117/12.445631.

[9] Ki-Nam Joo et al. "Simple heterodyne laser interferometer with subnanometer periodic errors". In: *Optics letters* 34.3 (2009), pp. 386–388. DOI: 10.1364/ol.34.000386.

[10] Peng-cheng Hu et al. "Balanced plane-mirror heterodyne interferometer with subnanometer periodic nonlinearity". In: *Applied optics* 53.24 (2014), pp. 5448–5452.

[11] Arjan JH Meskers, Jo W Spronck, and Robert H Munnig Schmidt. "Heterodyne displacement interferometer, insensitive for input polarization". In: *Optics letters* 39.7 (2014), pp. 1949–1952.

[12] Chien-ming Wu, John Lawall, and Richard D Deslattes. "Heterodyne interferometer with subatomic periodic nonlinearity". In: *Applied optics* 38.19 (1999), pp. 4089–4094.

[13] C Sternkopf et al. "Heterodyne interferometer laser source with a pair of two phase locked loop coupled He–Ne lasers by 632.8 nm". In: *Measurement Science and Technology* 23.7 (2012), p. 074006. DOI: doi:10.1088/0957-0233/23/7/074006. URL: http://iopscience.iop.org/0957-0233/23/7/074006.

[14] Stephan Georges et al. "Development of an integrated guiding and actuation element for high dynamic nanopositioning systems". In: *59th Ilmenau Scientific Colloquium*. (Technische Universität Ilmenau). Sept. 11, 2017.

CONTACTS

M.Sc. Oliver Dannberg oliver.dannberg@tu-ilmenau.de
Dipl.-Ing. Ingo Ortlepp ingo.ortlepp@tu-ilmenau.de